Electronic Supplementary Material (ESI) for Journal of Materials Chemistry A.

Supporting Information: Strain-modified ionic conductivity in rare-earth substituted ceria: Effects of migration direction, barriers, and defect-interactions

George F. Harrington,*[a,b,c,d] Sunho Kim,[c] Kazunari Sasaki,[a,b,d] Harry L. Tuller,[c,d] and Steffen Grieshammer,**[e,f,g]

[a] *Next-Generation Fuel Cell Research Centre, Kyushu University, Japan*
[b] *Center of Coevolutionary Research for Sustainable Communities (C^2RSC), Kyushu University, Japan*
[c] *Department of Materials Science and Engineering, Massachusetts Institute of Technology, USA*
[d] *International Institute for Carbon-Neutral Energy Research (WPI-I^2CNER), Kyushu University, Japan*
[e] *Helmholtz-Institute Münster (HIMS), IEK-12, Forschungszentrum Jülich, Germany*
[f] *Institute of Physical Chemistry, RWTH Aachen University, Germany*
[g] *JARA-HPC, Germany, Forschungszentrum Jülich & RWTH Aachen University, Germany*

* *E-mail: harrington.frederick.george.302@m.kyushu-u.ac.jp*
** *E-mail: s.grieshammer@fz-juelich.de*

1 Structural characterisation of RE:CeO_2 films

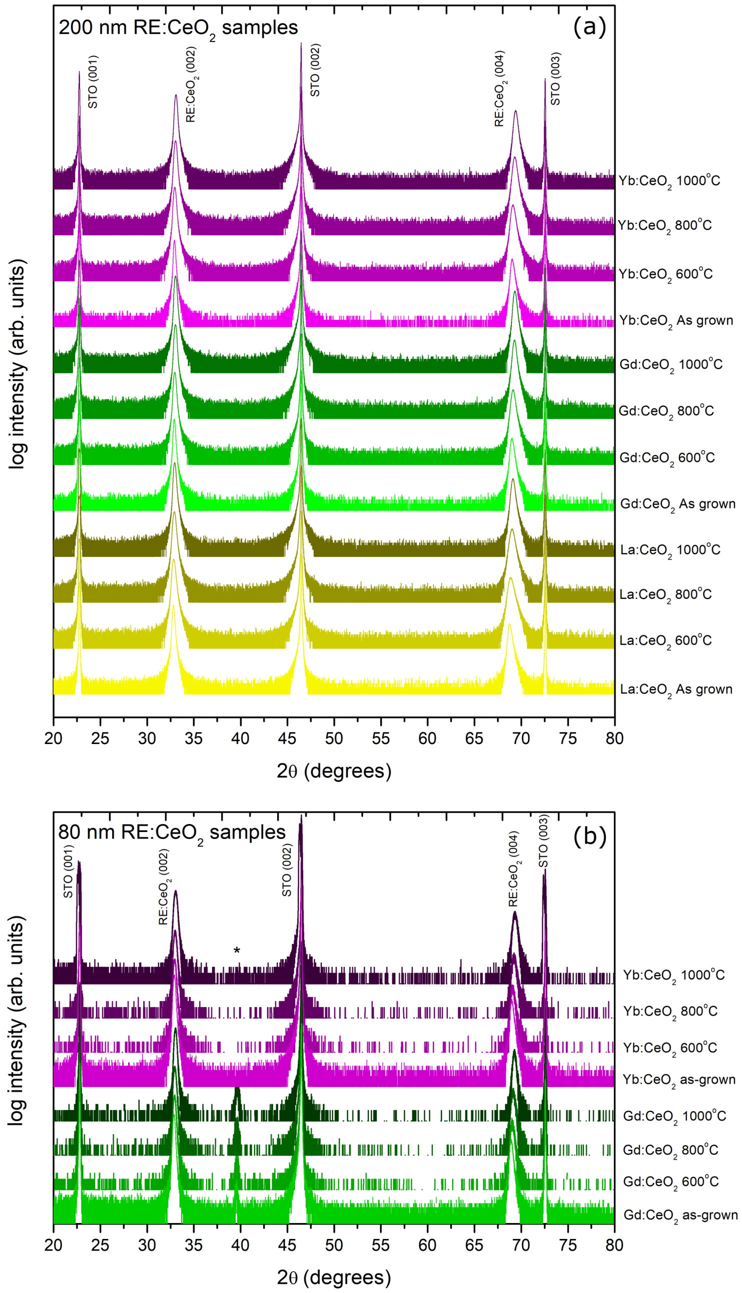

Figure S1: Out-of-plane XRD $2\theta/\omega$ scans of the (a) 200 nm thick samples and (b) 80 nm thick samples after annealing.

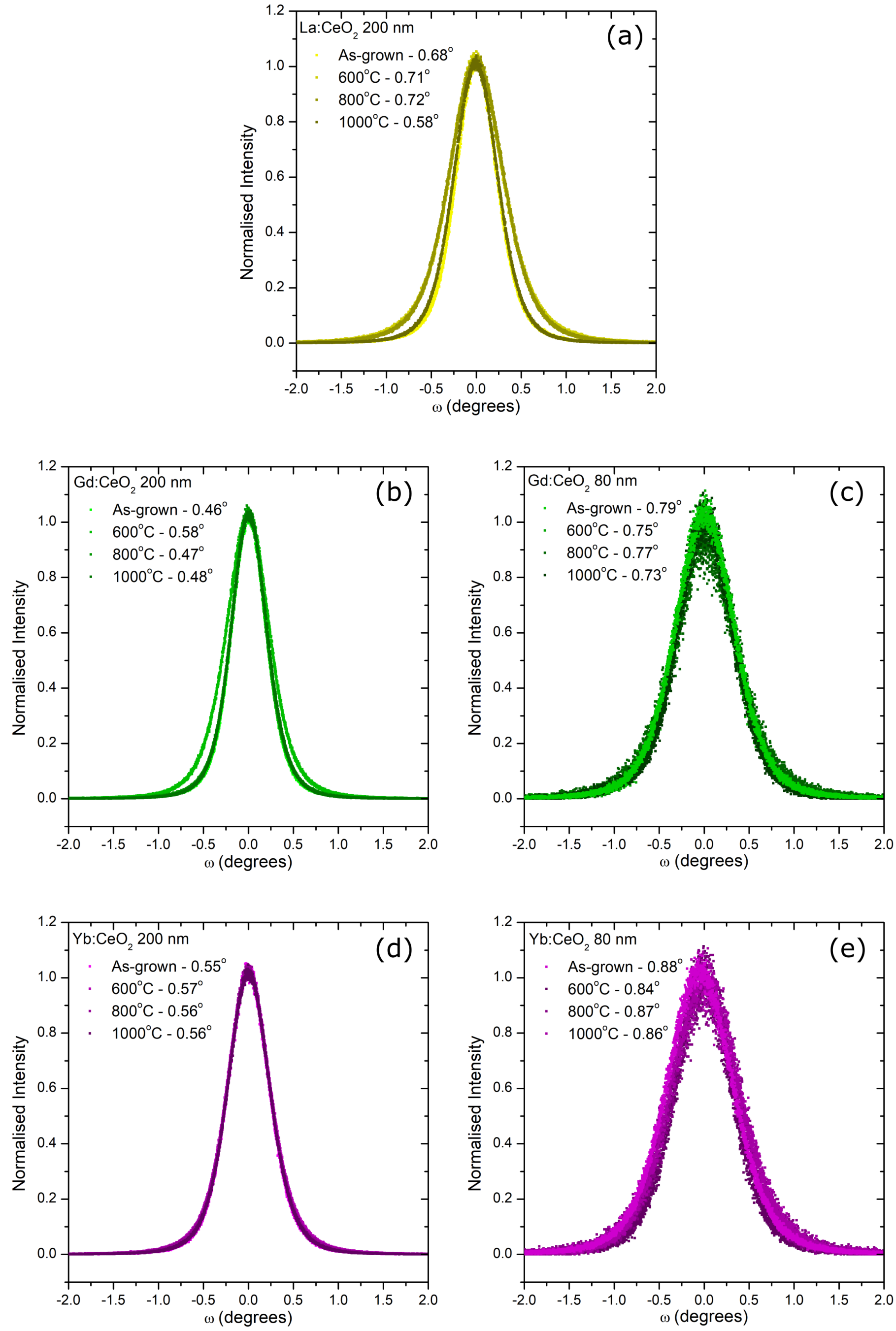

Figure S2: XRD rocking curves of the RE:CeO_2 002 peak from (a) 200 nm thick La:CeO_2 samples, (b) 200 nm thick Gd:CeO_2 samples, (c) 80 nm thick Gd:CeO_2 samples, (d) 200 nm thick Yb:CeO_2 samples, (e) 80 nm thick Yb:CeO_2 samples.

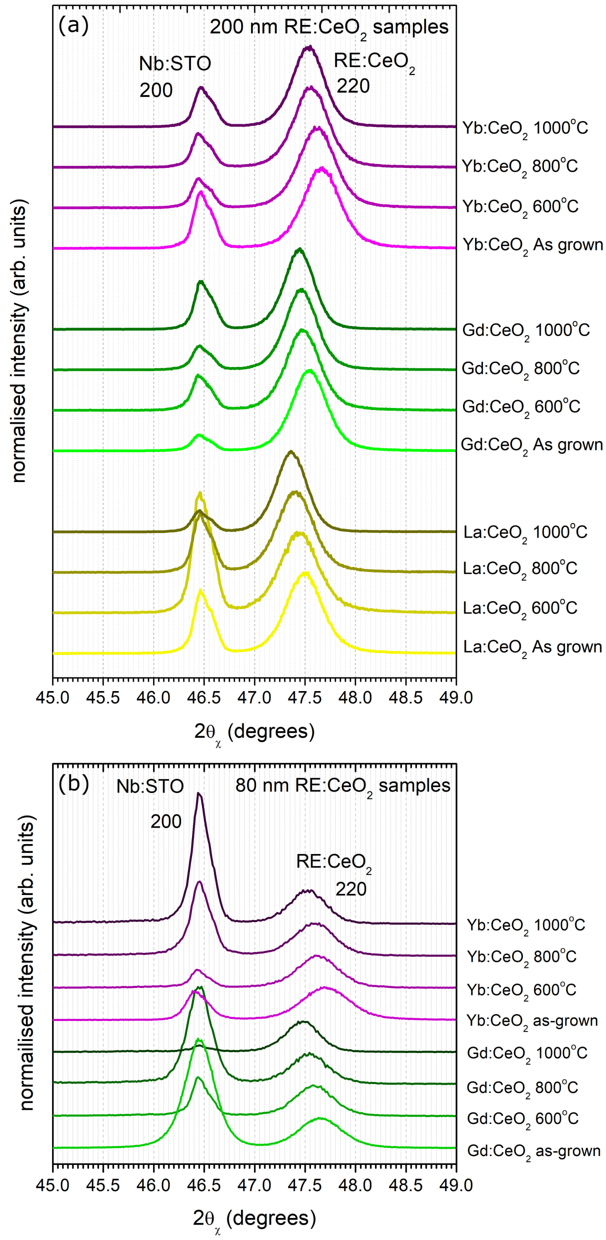

Figure S3: In-plane XRD $2\theta_\chi/\phi$ scans of the (a) 200 nm thick samples and (b) 80 nm thick samples after annealing.

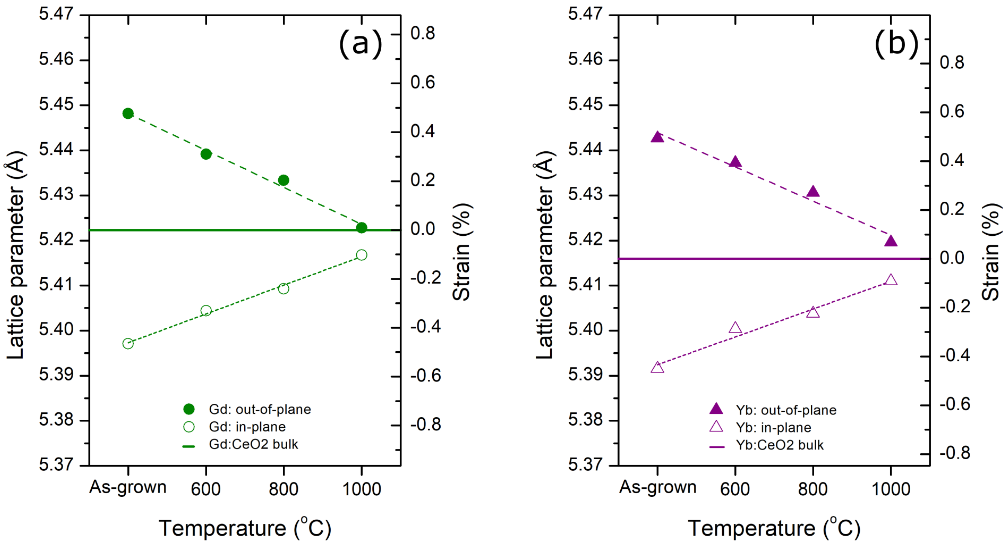

Figure S4: Lattice paramters of the (a) 80 nm thick Gd:CeO_2 samples and (b) 80 nm thick Yb:CeO_2 samples.

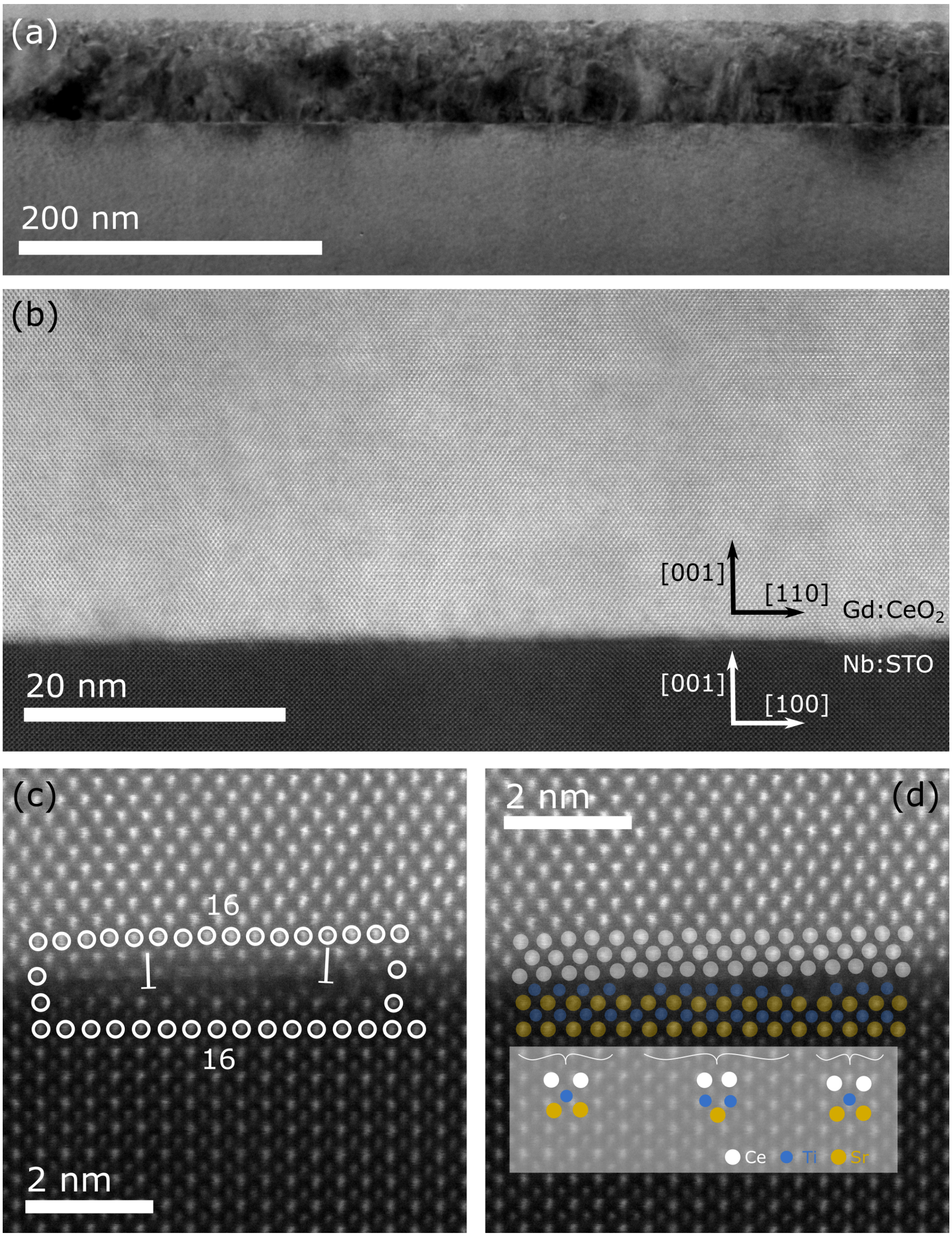

Figure S5: TEM micrographs of a 80 nm thick Gd:CeO_2 sample. (a) Bright-field TEM micrograph of the film where contrast variations in the substrate at the film/substrate interface can be observed which are attributed to strain surrounding interfacial dislocations. (b) High-resolution high-angle annular dark-field scanning TEM (HAADF-STEM) micrograph. (c) Magnified image of the film/substrate interface showing the Burgers circuit surrounding misfit dislocations. (d) The same micrograph as (c) with the position of Ce, Sr, and Ti atoms marked showing a change in interfacial structure at different regions.

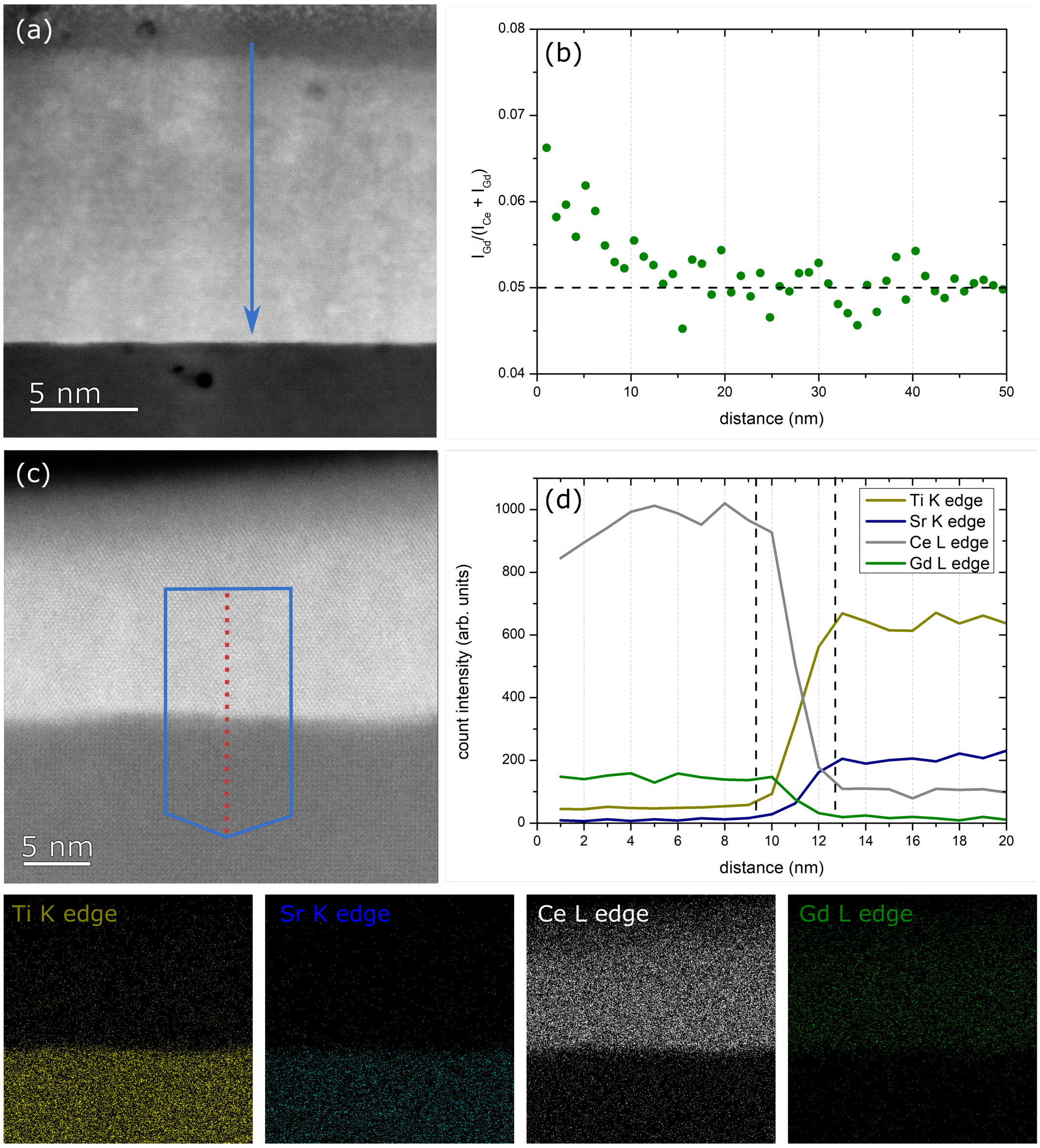

Figure S6: Analytical scanning transmission electron microscopy of the surface and substrate interface of a Gd:CeO_2 film after annealing at 1000°C. (a, b) shows a HAADF-STEM image and an electron energy loss spectroscopy (EELS) line-scan revealing Gd enrichment at the surface calculated from the Gd $M_{4,5}$ and Ce $M_{4,5}$ edges. Due to sample drift and poor signal-to-noise ratio, the analysis should be viewed as providing a general trend rather than exact quantification. (c, d) shows an X-ray energy dispersive spectroscopy (XEDS) line-scan across the Gd:CeO_2/Nb:STO interface along with elemental maps. An interfacial interdiffusion layer of approximately 3nm is identified, which is of the same order as the sample drift over the XEDS acquisition period. As such, we assume any interdiffusion is minimal.

2 Conductivity of RE:CeO$_2$ films

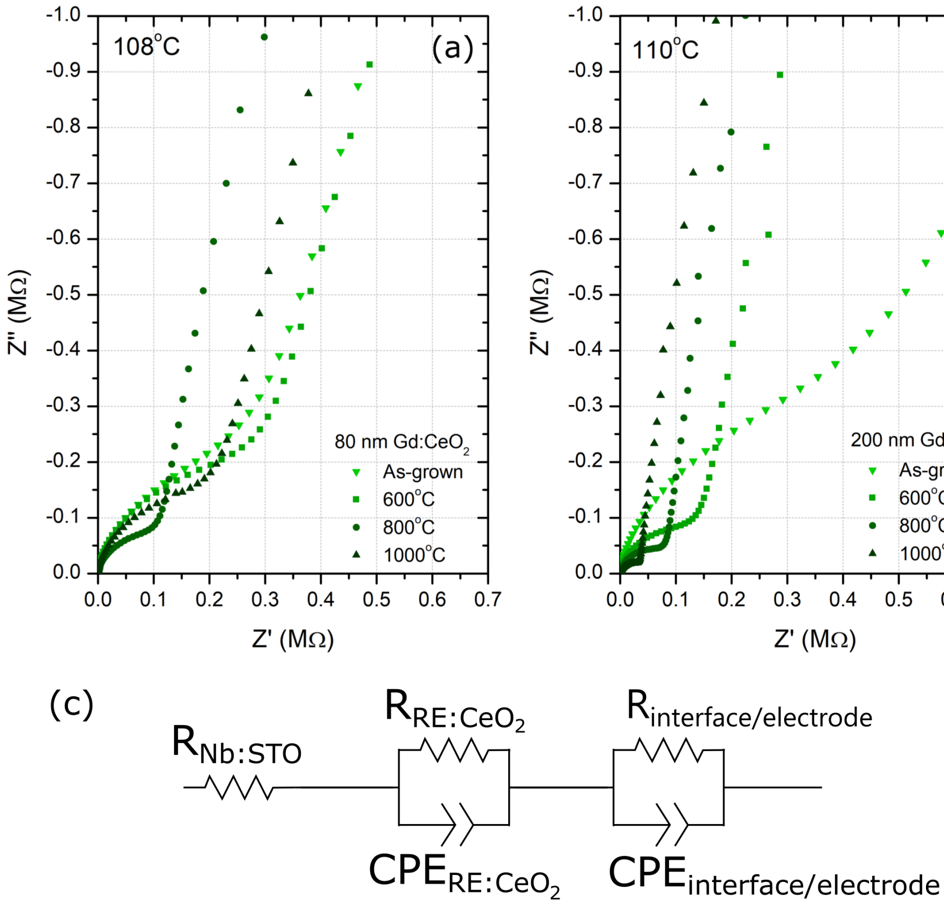

Figure S7: Representative Nyquist plots of the samples. (a) Nyquist plots of the 80 nm thick Gd:CeO$_2$ samples at ∼108°C. (b) Nyquist plots of the 200 nm thick Gd:CeO$_2$ samples at ∼110°C. (c) Equivalent circuit model used to fit the impedance spectra.

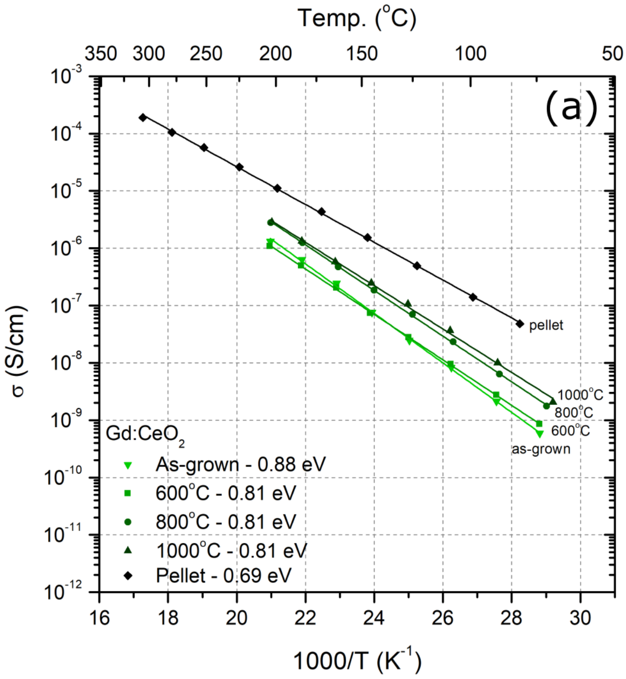

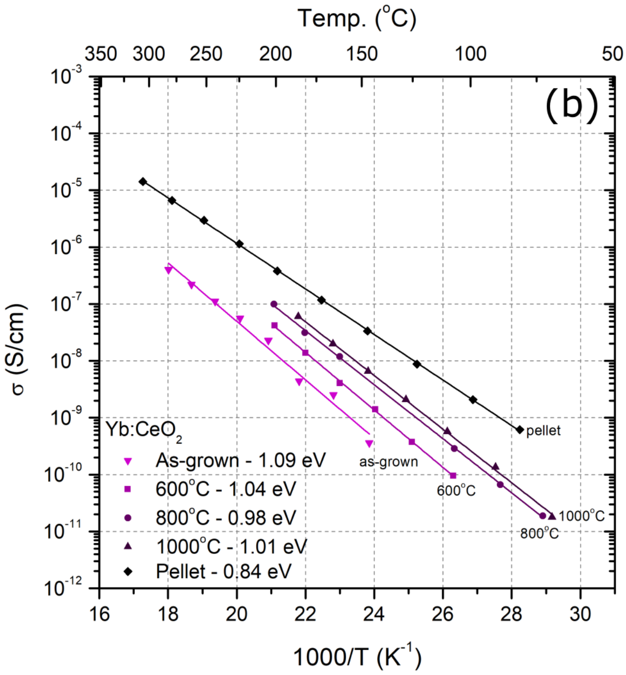

Figure S8: Arrhenius plots of the conductivity of the (a) 80 nm Gd:CeO_2 samples and (b) 80 nm Yb:CeO_2 samples with the bulk pellets for comparison. The activation energies are shown in the legend.

3 Information on samples

			Lattice parameters							
			out-of-plane		in-plane		volume		Conductivity	
Substituent	Thickness (nm)	Heat treatment (°C)	$c_{(002)}$ (Å)	Strain (%)	$a_{(220)}$ (Å)	Strain (%)	a^3 ($Å^3$)	Strain (%)	A_E (eV)	Ln σ_0
La	pellet	-	5.434	-	5.434	-	160.49	-	0.748	10.76
	200	as-grown	5.459	0.45	5.414	-0.37	160.02	-0.29	0.873	13.33
	200	600	5.453	0.34	5.420	-0.27	160.16	-0.20	0.865	13.77
	200	800	5.442	0.15	5.424	-0.19	160.11	-0.24	0.861	14.36
	200	1000	5.436	0.03	5.428	-0.12	160.17	-0.20	0.853	14.01
Gd	pellet	-	5.422	-	5.422	-	159.43	-	0.692	11.75
	80	as-grown	5.448	0.48	5.397	-0.47	158.70	-0.46	0.885	13.29
	80	600	5.439	0.31	5.404	-0.33	158.87	-0.35	0.809	12.05
	80	800	5.433	0.20	5.409	-0.24	158.98	-0.28	0.807	12.84
	80	1000	5.423	0.01	5.417	-0.10	159.11	-0.20	0.803	13.36
	200	as-grown	5.443	0.37	5.409	-0.25	159.22	-0.13	0.819	11.64
	200	600	5.435	0.24	5.416	-0.12	159.41	-0.01	0.791	13.04
	200	800	5.424	0.02	5.418	-0.09	159.18	-0.15	0.812	13.87
	200	1000	5.422	0.00	5.420	-0.05	159.26	-0.11	0.793	13.74
Yb	pellet	-	5.416	-	5.416	-	158.86	0.00	0.837	12.00
	80	as-grown	5.443	0.49	5.392	-0.45	158.21	-0.41	1.094	12.08
	80	600	5.437	0.39	5.400	-0.29	158.57	-0.18	1.040	12.05
	80	800	5.431	0.27	5.404	-0.22	158.58	-0.18	0.977	14.52
	80	1000	5.420	0.07	5.411	-0.09	158.68	-0.11	1.005	14.10
	200	as-grown	5.440	0.44	5.396	-0.37	158.38	-0.30	1.036	12.15
	200	600	5.435	0.35	5.401	-0.28	158.52	-0.21	0.999	12.89
	200	800	5.422	0.11	5.407	-0.16	158.52	-0.22	0.972	13.98
	200	1000	5.415	-0.01	5.410	-0.11	158.49	-0.24	0.952	14.03

Table S1: Details of the films in this study.

4 Calculation of the effect of a segregation layer on the out-of-plane conductivity

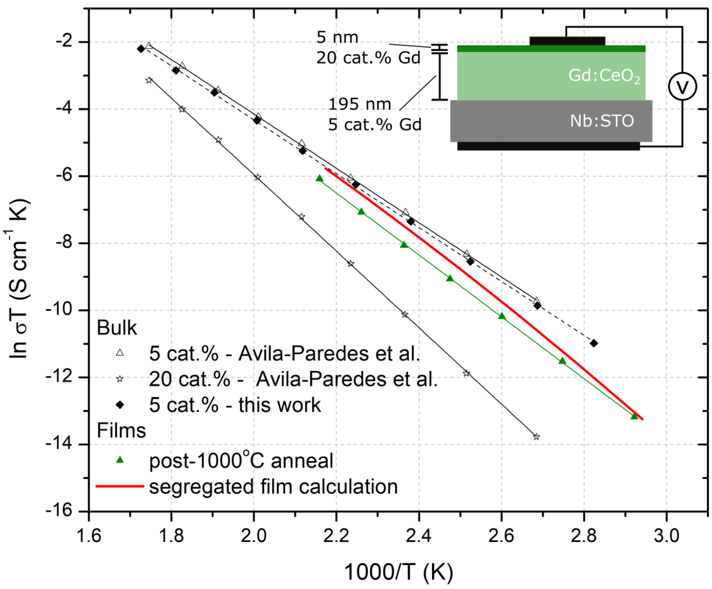

Figure S9: Calculation of expected out of-plane conductivity a 200nm thick 5cat.% Gd:CeO_2 film with a 5 nm thick 20cat.% Gd:CeO_2 segregation layer at the surface. The bulk (grain core) conductivity values are taken from Avila Paredes et al. [1] and also plotted. The bulk conductivity of the pellet used in this study, and a 200nm thick Gd:CeO_2 film sample after annealing at 1000°C are plotted for comparison. Values for the activation energies and preexponential factors are given in Table S2.

	E_a (eV)	Ln σ_0
5 cat.% - Avila Paredes et al.	0.698	12.06
20 cat.% - Avila Paredes et al.	0.983	16.85
5 cat.% - this work	0.692	11.75
post-1000°C film	0.795	13.80
composite film calculation	0.839	15.48

Table S2: Activation energies E_a and preexponential factors Ln σ_0 from Figure S9.

5 Density functional theory calculations

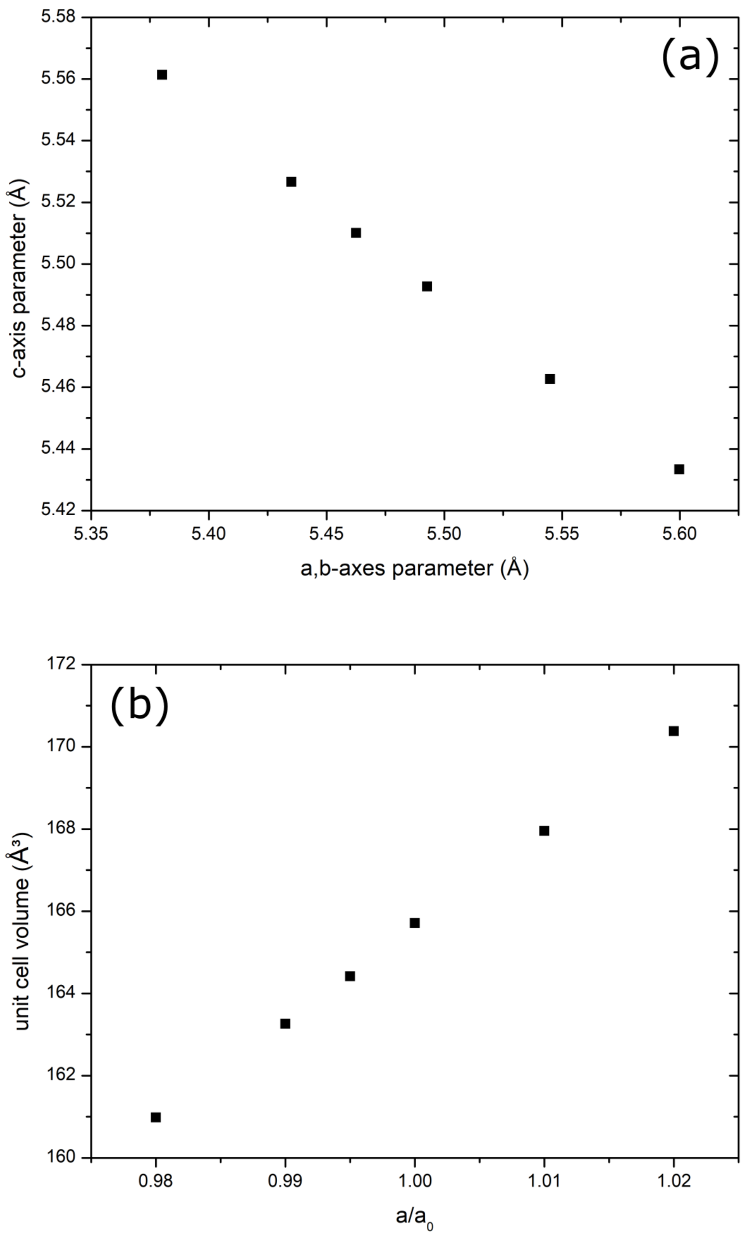

Figure S10: (a) Relation between the c-axis parameter and a,b-axes parameter of the unit cell. (b) Relation between the in-plane strain and unit cell volume.

$$\Delta E_{conf,v-v} = \alpha_{v-v} + \beta_{v-v} \cdot (a/a_0)$$

	$1NN^{in}$	$1NN^{out}$	$4NN^{in}$	$4NN^{out}$
α_{v-v}	8.718	-2.634	2.411	-2.979
β_{v-v}	-7.88	3.472	-2.149	3.241

Table S3: Strain dependence of the v-v interaction energy of the 1^{st} nearest neighbour (1NN) and 2^{nd} nearest neighbour (2NN) positions for both in-plane and out-of-plane directions.

$$\Delta E_{conf,RE-v} = \alpha_{RE-v} + \beta_{RE-v} \cdot (a/a_0)$$

	Lu	Gd	La
α_{RE-v}	-2.445	-1.833	-1.319
β_{RE-v}	2.05	1.625	1.256

Table S4: Strain dependence of the RE-v interaction energy of the 1^{st} nearest neighbour (1NN) position for Lu, Gd, and La.

$$\Delta E^{out}_{edge,AB} = \alpha^{out}_{edge,AB} + \beta^{out}_{edge,AB} \cdot (a/a_0)$$

	Ce-Ce	Lu-Ce	Gd-Ce	La-Ce	Lu-Lu	Gd-Gd	La-La
$\alpha^{out}_{edge,AB}$	9.37	7.74	9.87	12.96	7.19	11.33	17.39
$\beta^{out}_{edge,AB}$	-8.9	-7.29	-9.3	-12.19	-6.56	-10.43	-16.1

Table S5: Strain dependence of the edge energies for the out-of-plane migration direction.

$$\Delta E^{in}_{edge,AB} = \alpha^{in}_{edge,AB} + \beta^{in}_{edge,AB} \cdot (a/a_0) + \gamma \cdot (a/a_0)^2$$

	Ce-Ce	Lu-Ce	Gd-Ce	La-Ce	Lu-Lu	Gd-Gd	La-La
$\alpha^{in}_{edge,AB}$	-69.49	-68.38	-124.98	-128.01	-17.45	-76.9	-65.525
$\beta^{in}_{edge,AB}$	143.15	140.28	254	260.72	37.37	156.89	136.31
$\gamma^{in}_{edge,AB}$	-73.2	-71.45	-128.45	-131.95	-19.3	-79.1	-69.5

Table S6: Strain dependence of the edge energies for the in-plane migration direction.

6 Kinetic Monte Carlo calculations

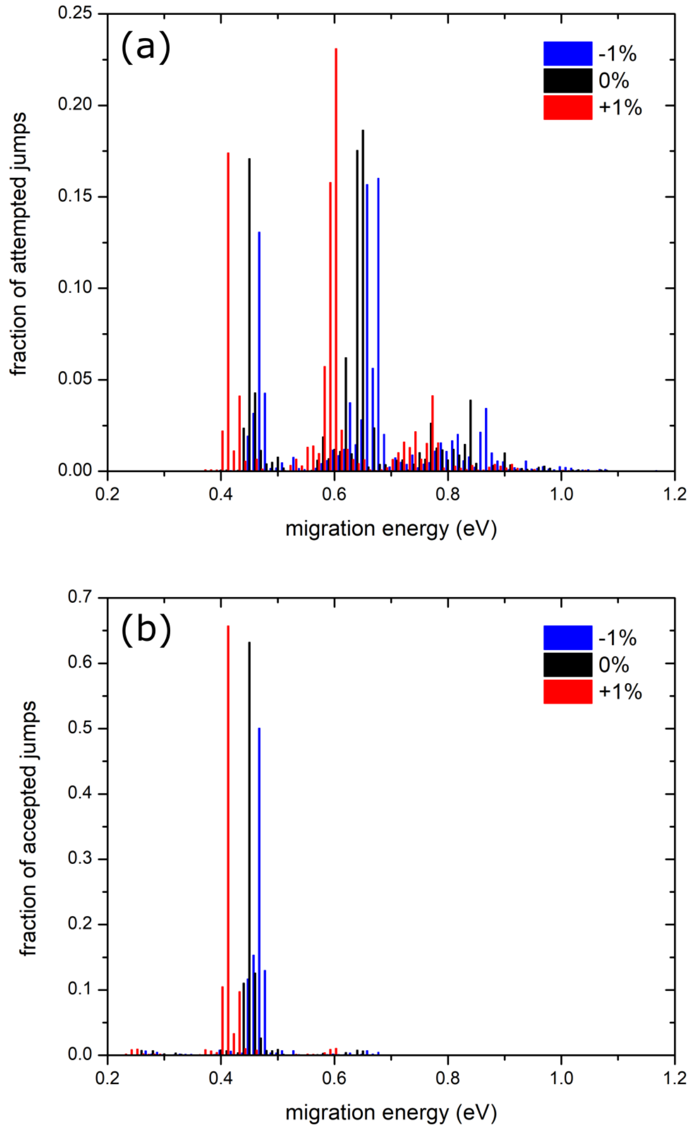

Figure S11: Fraction of the (a) attempted and (b) successful in-plane jumps for Lu:CeO_2 for different strains.

References

[1] Hugo J. Avila-Paredes, Kwanghoon Choi, Chien-Ting Chen, and Sangtae Kim. Dopant-concentration dependence of grain-boundary conductivity in ceria: A space-charge analysis. *Journal of Materials Chemistry*, 19(27):4837, 2009.